Adjoint-Based Optimization on the Hydrodynamic Performance of Flexible Swimmers

Bolun Xu*, Daniel Colgan[†] and Mingjun Wei[‡] *Kansas State University, Manhattan, KS 66506*

John Hrynuk[§]
DEVCOM Army Research Lab, Aberdeen Proving Ground, MD 21005

In this work, an adjoint-based approach is developed and implemented to optimize the hydrodynamic force on multiple flexible swimmers in laminar incoming flow for the first time. Two-dimensional (2D) flexible hydrofoils arranged in tandem and diamond formation are studied in the present paper. The horizontal hydrodynamic force on the following swimmers is first optimized by controlling the heaving and undulatory motion, then further optimized by controlling the position of following swimmers. A weight function is introduced to allow for optimization on multiple objectives. It is found that for the triple-swimmer case, the drag-to-thrust conversion can be achieved on both following swimmers by triggering heaving motion and tuning the wave length of undulation. Formation optimization results in wider distance between the leading swimmer and the 2nd swimmer, with both following swimmers positioned closer to each other. For the quadruple-swimmer case, the motion optimization increases the heaving motion and modifies the wave length of undulation, which reduces the drag on the 2nd and the 3rd swimmer, while converting drag to thrust for the 4th swimmer. The formation optimization is also find to move the 2nd and 3rd swimmer farther from the leading swimmer, while positioning the 4th swimmer closer to the swimmers ahead. Further analysis on vortex structures indicates that the following swimmers tend to avoid the direct impingement of vortices from the swimmer ahead. In addition, they are able to take advantage of more active interactions between separation vortices and the wake from swimmers ahead, to benefit from suction effect for the thrust enhancement. The results achieved in this work can shed some light on the mechanism of hydrodynamic benefits brought by the interactions between flows and flexible swimmers.

Nomenclature

p = pressure

 ρ = density of solid body

u = flow velocity Ω = fluid domain $\partial \Omega_s$ = solid boundary δ = Kronecker delta Re = Reynolds number St = Strouhal number v = kinetic viscosity

t = dimensional simulation time

L = horizontal distance between neighboring swimmers
 H = vertical distance between neighboring swimmers

 U^* = incoming flow velocity A = heaving amplitude

^{*}Ph.D., Alan Levin Department of Mechanical and Nuclear Engineering, Member AIAA

[†]Master, Alan Levin Department of Mechanical and Nuclear Engineering, Student Member AIAA

[‡]Associate Professor, Alan Levin Department of Mechanical and Nuclear Engineering, Associate Fellow AIAA

[§] Research Mechanical Engineer, DEVCOM Army Research Lab, Member AIAA

 λ = wave length of undulation δx = horizontal displacement δy = vertical displacement

 Δt = time step for direct simulation and adjoint-based optimization

 \mathcal{J} = objective function

w = weight in the objective function

g = gradient function γ = control vector C_D = drag coefficient

 C_{Fx} = horizontal force coefficient

 C_T = thrust coefficient

Superscripts

* = adjoint variables or operators (except for U^*)

I. Introduction

It has long been hypothesized that the swimming animals may be able to make use of flows induced by neighboring swimmers when schooling, to obtain hydrodynamic benefits, including the drag reduction, the thrust and the propulsion efficiency enhancement 1-3. Extensive work has been done attempting to elucidate the mechanisms of possible benefits brought by schooling, as well as to seek the ways of schooling that can lead to better hydrodynamic performance. Some pioneering work has been conducted by using living fish and fish-like robotics, which has indicated that through the collective motion and vortex phase matching, individuals in a fish school can achieve hydrodynamic benefits such as lower energy consumption 4.6. However, since the number of swimmers in a fish school is usually huge, the interactions between swimmers and surrounding flows are very complicated, which makes it difficult to thoroughly analyze the hydrodynamic performance by merely studying living fish school. Therefore, fish schooling has usually been studied using simplified models. Some work has modeled the fish school as self-propelled particles, which can only take into account limited hydrodynamics [7]. In order to further investigate the complex hydrodynamic interaction of fish schooling, more work has been focusing on models consisting of moving foils and fins with different arrangements of formations [9-13]. The flexible undulatory hydrofoil model has been widely used to numerically investigate the schooling behavior of swimmers. This model is derived from the spine motion of fish [8], and has been widely used to study the effects of spatial arrangement of the fish and features of tail beating on the hydrodynamic performance of fish schooling [9-13]. In general, the hydrodynamic performance of schooling has been found highly dependent on the motion of each fish (i.e., flapping, undulating, etc.), as well as the spacing or the formation of the fish. These two major factors are reviewed as follow.

Using the flexible swimmers model, Gao and Triantafyllou [9] studied the effect of swimmer's caudal fin pitching on the reduction of self-propulsion energy in the wake of an upstream swimmer. Park and Sung [10] studied the schooling behavior of flexible fins by adding transverse heaving motion on the leading edge of each fin, while the body is passively driven by the surrounding fluid to undulate. It was found that the following swimmers were able to reduce the heaving amplitude to optimize their propulsive efficiency regardless whether they were schooling in triangle or diamond formation.

The geometrical arrangements of formation and the spacing distance between swimmers have also been found to play important roles in the hydrodynamic performance of schooling. For the flexible swimmer model, Hemelrijk et al. [14] numerically studied various schooling configurations, and suggested the optimal lateral distance for a diamond formation was 1.6 times the body length (BL) of swimmer. Daghooghi and Borazjani [15] studied a rectangular formation with 3D numerical simulation and found the optimal power efficiency can be achieved with lateral distance equal to 0.4 BL. Recently, high-fidelity DNS was conducted by Pan and Dong [11] to investigate the density effect of a diamond formation on the hydrodynamic performance of schooling. It was found that dense school can achieve higher thrust production as well as higher propulsive efficiency. The lower spacing induced a wall effect to generate an angled jet, which eventually benefitted the thrust production.

Despite ample studies having been conducted on the complex flow interactions of schooling, no study has demonstrated the conclusive reasoning for schooling behaviors. Moreover, the optimal motion or formation of swimmers that correspond to the optimal hydrodynamic performance is still too difficult to achieve using current numerical or

experimental approaches, because of the huge parametric space a fish school can have. Recently, Ji et al. [16] proposed leveraging an active learning method to optimize the propulsion performance. Nonetheless, the data training was still computationally expensive which may limit the size of parametric space the method can feasibly explore. Additionally, deep learning based approaches often struggle to provide comprehensive physical understandings of fluid flows.

As a different route, an adjoint-based approach is able to handle a large number of control parameters simultaneously without significantly increasing the computational cost, as reviewed and used in previous chapters. Therefore it became a natural choice to optimize the hydrodynamic performance of swimmer schooling with both motion and formation being taken into account. The hydrodynamic performance was evaluated by the horizontal forces (i.e., drag or thrust) on following hydrofoils. For convenience, hereafter in this paper "swimmers" will also be used to refer to hydrofoils. Both rigid and flexible swimmer models were studied for optimized swimmer motion and formation to achieve lowest drag or highest thrust at low Reynolds numbers. The adjoint-based approach was implemented with full-order model (FOM) simulated by solving incompressible Navier-Stokes equation. The remainder of this chapter is outlined as follows. Section introduces the numerical methods and computational configurations. The results of optimal schooling for flexible swimmers are presented in section with the discussion on flow physics. Section varieties of this work.

II. Methodology

A. Governing equations

The flow is governed by the incompressible Navier-Stokes equation. In order to resolve the moving solid boundary, the immersed boundary method (IBM) with direct forcing is used here to represent the solid boundary conditions [17] [18]:

$$\frac{\partial \mathbf{u}}{\partial t} + (\mathbf{u} \cdot \nabla)\mathbf{u} = -\nabla p + \frac{1}{Re} \nabla^2 \mathbf{u} + \mathbf{f},\tag{1}$$

where Re is the Reynolds number. The forcing term f can be nominally expressed by:

$$f = \begin{cases} [(\boldsymbol{u} \cdot \nabla)\boldsymbol{u} - \frac{1}{Re}\nabla^2\boldsymbol{u}]^n + \frac{1}{\Delta t}(\boldsymbol{\gamma} - \boldsymbol{u}^n), & \text{in } \partial\Omega_s \\ 0, & \text{otherwise,} \end{cases}$$
 (2)

where the superscript n denotes the variables at n-th time step, Δt is the size of time step in DNS discretization, γ is the prescribed velocity of the solid body, which is introduced as the control parameter. By solving Eq. [1] high-fidelity solutions of the flow field can be obtained. The solving process and numerical method were introduced in our previous works[19-21], where it was successfully implemented in flows with a single solid body. In this work, the in-house code has been extended to resolve flows with arbitrary number of solid bodies, which greatly improved its ability to simulate more complex fluid-structure interactions.

B. Adjoint equation and objective function

The main goal of this work is to optimize the horizontal hydrodynamic force on swimmers. Therefore, the objective function \mathcal{J} is defined accordingly as:

$$\mathcal{J} = \frac{1}{TD_0} \int_T \int_{\partial \Omega_c} \sigma_{1j} n_j ds dt, \tag{3}$$

where $D_0 = 1/2\rho U^{*2}D$, σ is the viscous stress, T is one period of solid oscillation, and subscript "1" represents the horizontal direction. Note that during the optimization, a positive \mathcal{J} represents the drag, and a negative \mathcal{J} represents the thrust. The adjoint approach enabled by the non-cylindrical calculus toolbox was used here [20-23]. Within this framework, the adjoint equation $\mathcal{N}^*(q)q^* - \mathcal{F}^* = 0$ based on the objective function (Eq. 3) is given as:

$$\mathcal{N}^{*}(\boldsymbol{q})\boldsymbol{q}^{*} = \begin{bmatrix} \frac{\partial u_{j}^{*}}{\partial x_{j}} \\ \frac{\partial u_{i}^{*}}{\partial t} + u_{j}(\frac{\partial u_{i}^{*}}{\partial x_{j}} + \frac{\partial u_{j}^{*}}{\partial x_{i}}) + v \frac{\partial^{*} u_{i}^{*}}{\partial x_{j}^{2}} + \frac{\partial p^{*}}{\partial x_{i}} \end{bmatrix},$$

$$\mathcal{F}^{*} = 0, \quad \text{in} \quad \Omega$$

$$u_{i}^{*} = -\delta_{1i}, \quad \text{on} \quad \partial \Omega_{S}.$$

$$(4)$$

And the adjoint equation for transverse map velocity variable Z is:

$$Z_i^* = -(\sigma_{ii}^* n_j + u_i^* u_i n_i) \quad \text{on} \quad \partial \Omega_s.$$
 (5)

By solving adjoint Eq. $\boxed{4}$ and Eq. $\boxed{5}$ the gradient g can be obtained as:

$$g = \frac{1}{TD_0} \int_T \int_{\partial \Omega_s} Z_k \left(-\frac{dZ_k^*}{dt} - Z_k^* \operatorname{div}_{\partial \Omega_s} \gamma - Z_i^* \frac{\partial u_i}{\partial x_k} + \frac{\partial \sigma_{1j}}{\partial x_j} n_k \right) ds dt.$$
 (6)

The above derivation is focused on the optimization of a single solid body. However, in the current study, it is more practical to consider the hydrodynamic performance of all solid bodies of interest at the same time. This was accomplished by introducing a weight w_i for each solid body of interest in the present work, where $w_i \in [0, 1]$ and $\sum_i w_i = 1$. With w_i multiple objectives might be optimized by the modified \mathcal{J} :

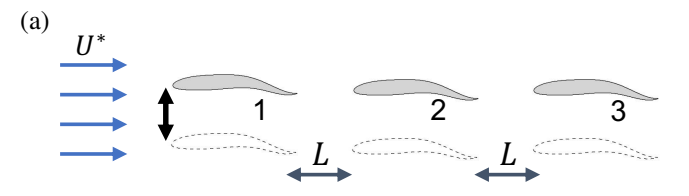
$$\mathcal{J} = \sum_{i} w_{i} \mathcal{J}_{i},\tag{7}$$

where \mathcal{J}_i has the form of equation 3. The gradient is modified accordingly as:

$$g = \sum_{m} w_{m} \frac{1}{TD_{0}} \int_{T} \int_{\partial\Omega_{s,m}} Z_{k,m} \left(-\frac{dZ_{k,m}^{*}}{dt} - Z_{k,m}^{*} \operatorname{div}_{\partial\Omega_{s,m}} \gamma - Z_{i,m}^{*} \frac{\partial u_{i}}{\partial x_{k}} + \frac{\partial \sigma_{1j}}{\partial x_{j}} n_{k}\right) ds dt.$$
 (8)

C. Swimmer models and computational setup

The 2D simulation was performed on a rectangular computational domain of $40c \times 20c$, where c was the chord length of each hydrofoil. The domain was discretized by a 1001×501 non-uniform Cartesian mesh, with minimum mesh size $\Delta x_{\min} = 1.5 \times 10^{-2}c$. The mesh was refined and uniform in the near field of all hydrofoils in a $9c \times 6c$ area, and gradually coarsened towards the far field. In the present work, a flexible swimmer model was considered, as shown in figure T. Each swimmer initial has an NACA0012 shape, and is able to heave vertically, and to undulate along



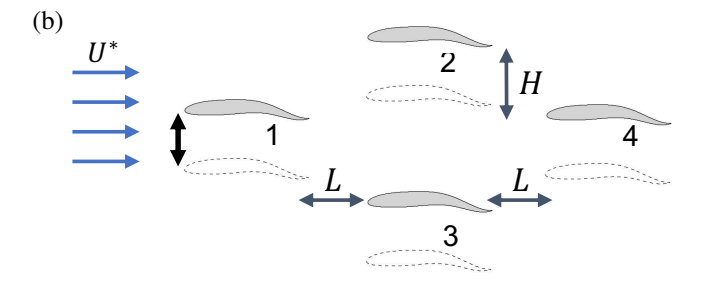


Fig. 1 The illustrations of swimmer models studied in the present work, each swimmer can heave vertically and have the carangiform undulating motion. (a): Three swimmers in tandem formation; (b): four swimmers in diamond formation. Numbers are used in following sections to refer to corresponding swimmers.

its center line at the same time. This model has been widely used previously $\boxed{3}$ $\boxed{1}$ $\boxed{3}$ $\boxed{24}$, to mimic the fish-like swimming by introducing prescribed traveling wave kinematics on the swimmer. The horizontal tip-to-tail distance between neighboring swimmers is denoted as L. For the diamond formation, the vertical distance between the upper (or the lower) swimmer and the leading swimmer is denoted as H. The present study was to optimize the schooling of

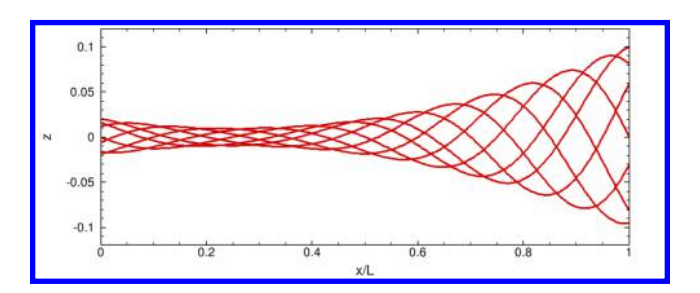


Fig. 2 Traveling wave amplitude of a carangiform motion at different time moments in one undulatory period.

multiple swimmers following a leading swimmer, where the leading swimmer was moving on its own regardless of the motion and location of followers, while all followers need to adjust their motion or location to gain hydrodynamic benefits. Therefore, the control was only enforced on followers.

Similar to some previous work [11, 24, 25], the carangiform undulating motion was modeled for each swimmer in the present work. The following traveling wave function was used to prescribe the undulation:

$$z(x,t) = P(x) \cdot \sin[2\pi(\frac{x}{\lambda} - ft)],\tag{9}$$

where the position variables, x and z, are normalized by c already. Therefore locally x=0 denotes the leading edge of the hydrofoil and x=1 is the trailing edge. This wave function expresses the undulating motion of the midline of the hydrofoil, which can be regarded as the spine of swimmers. So z(x,t) represents the lateral deviation of any point on the midline of the body at time moment t. λ is the wavelength of the traveling wave over an undulating body, which will be controlled. P(x) is the amplitude envelope of a lateral motion and has a quadratic polynomial form:

$$P(x) = a_2 x^2 + a_1 x + a_0, (10)$$

where $a_0 = 0.02$, $a_1 = -0.0825$, $a_2 = 0.1625$ as measured in experiments for carangiform motion [26]. The amplitude envelope of carangiform motion used in the present work is presented in figure 2 for different time moments in a tail-beat period. Besides undulation, the vertical heaving motion as well as the formation of following swimmers will also be studied for the flexible swimmer model, which can be described by:

$$X_i(t) = \delta x_i,$$

$$Y_i(t) = A_i \sin(2\pi f t) + \delta y_i,$$
(11)

where δx_i and δy_i are the horizontal and vertical displacement of each swimmer respectively. The oscillating frequency f was fixed to 0.2 for all cases in the present work. Combining Eq. 9 and Eq. 11, the control vector of each follow is given as $\gamma_i = [A_i, \lambda_i, \delta x_i, \delta y_i]$, of which the total dimension of the control is up to 4 for each of the following swimmers.

III. Results and Discussion

A. Three swimmers in tandem formation

In this section, three flexible swimmers were initially performing harmonic undulation governed by Eq. $\boxed{9}$ at Re=200 in tandem formation as illustrated in figure $\boxed{1}$ (a), with horizontal spacing L=0.5c. The swimmers were able to heave freely in vertical direction as well. The control was focused on motion first, then based on the optimal motion, an optimization on the position was carried out. Both optimizations were aimed at optimizing the horizontal force on the following two swimmers, to either minimize the drag or maximize the thrust. For the optimization on motion the control parameters were $\gamma_i = [A_i, \lambda_i]$ with i=2,3, leading to 4 control parameters in total. For the initial synchronous undulation, all three swimmers had the same $\gamma_i^{(0)} = [0, 1.0]$. A snapshot of the initial flow field is presented in figure $\boxed{3}$ A_i was limited in a range of [-1,1], and the wave length λ_i was constrained in a range of [0.1,2]. All force coefficients were averaged in one undulating period with T=5. With only undulation, initially flow attached onto three swimmers with no shedding vortex forming in the wake. The two followers initially had net mean drag as $C_{D2} = 0.122$ and $C_{D3} = 0.104$.

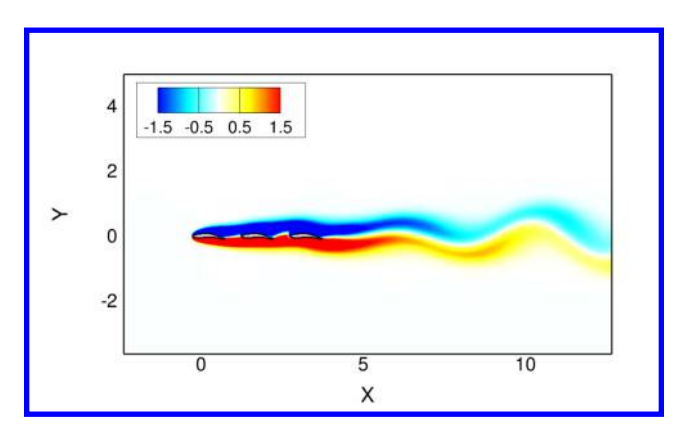


Fig. 3 The flow field of triple flexible swimmers undulating synchronously in tandem formation contoured by vorticity.

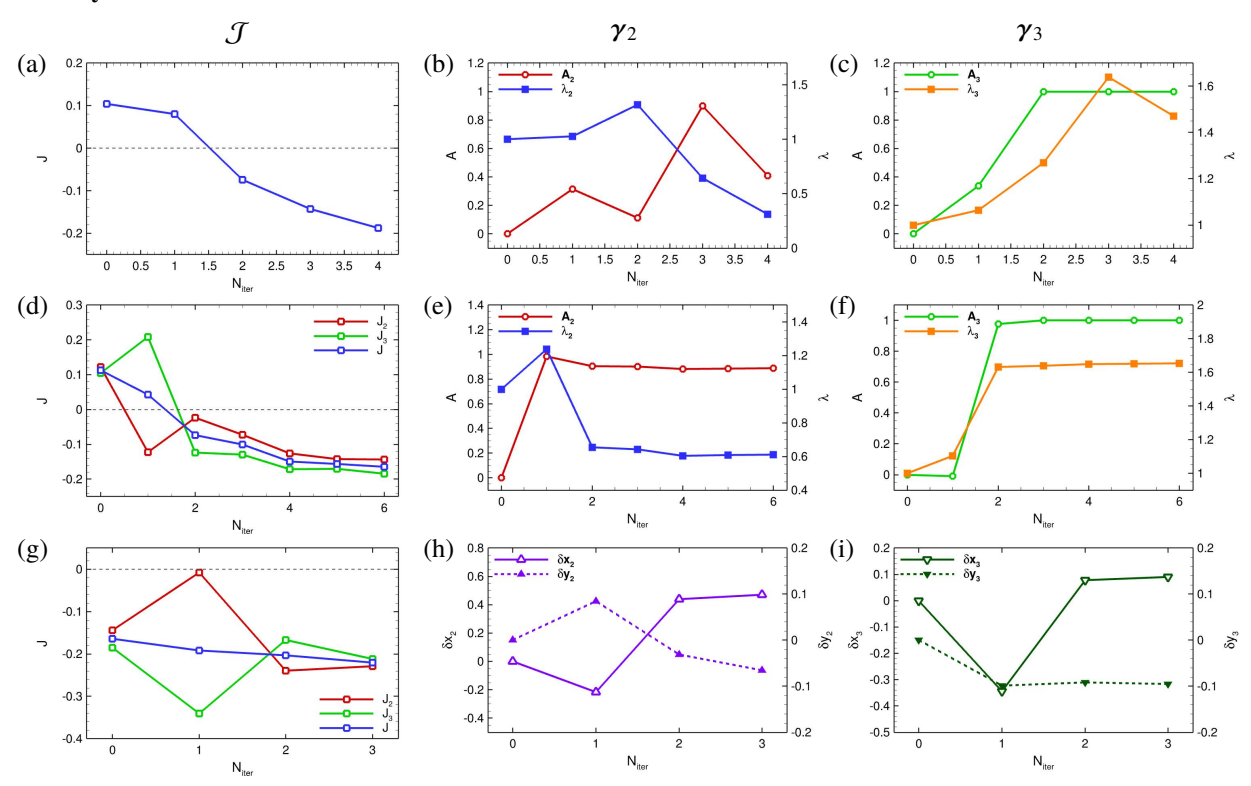


Fig. 4 The variations of objective function \mathcal{J} (left column), γ_2 (mid column) and γ_3 (right column) with respect to optimization iterations. (a – c): motion optimization with w = [0, 0.5, 0.5]; (d – f): motion optimization with w = [0, 0.5, 0.5]; (g – i): formation optimization with w = [0, 0.5, 0.5].

The variations of \mathcal{J} and γ_i during the motion optimization are shown in figure $\boxed{4}$. Two different weights were used to construct \mathcal{J} . The first case had a weight w=[0,0,1] which only optimized the 3rd swimmer. The second case had equal weight on both following swimmers with w=[0,0.5,0.5]. It can be seen that when only the 3rd swimmer was controlled, C_{D3} was effectively reduced by 279%, then eventually converted to a net thrust equal to $C_T=0.187$. However, C_{D2} was conversely increased by 12.3% to $C_{D2}=0.137$, which indicates that when optimizing exclusively for the third swimmer, performance of the second swimmer is sacrificed. The heaving amplitude of both following swimmers increased drastically, as $A_2=0.41$ and $A_3=1.0$, which was the upper limit set for heaving amplitude. The wave length of the undulation also altered, with λ_2 decreased by 68.9% and λ_3 increased by 47.1%. When both following swimmers were controlled, γ changed differently yet with the similar trend to achieve optimal hydrodynamic

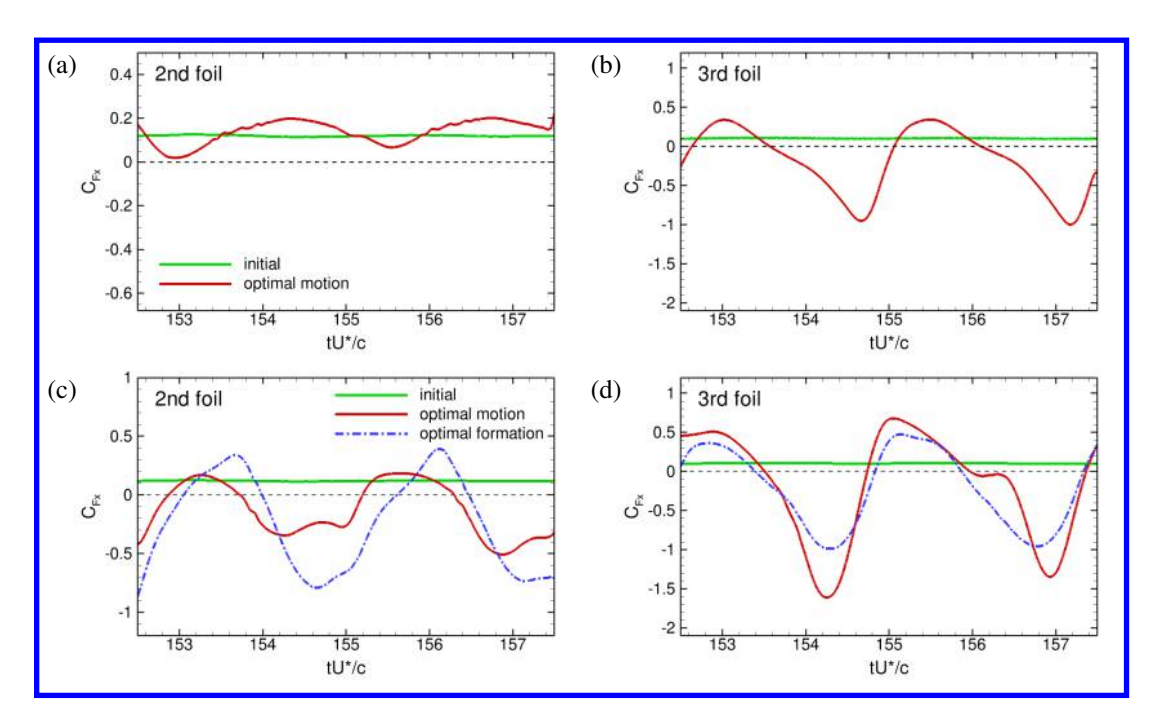


Fig. 5 The horizontal force coefficient profile in one undulating period before and after motion and formation optimization for the 2nd (left column) and the 3rd (right column) swimmer. (a - b): w = [0, 0, 1]; (c - d): w = [0, 0.5, 0.5].

performance as indicated in figure $\boxed{4}$ (d – f). In terms of heaving motion, both A_2 and A_3 were increased to 0.88 and 1.0 respectively. The 2nd swimmer had to heave more actively to achieve higher thrust. While for the undulation, λ_2 decreased by 39.0% and λ_3 increased by 65.2%. By conducting optimal motion, both following swimmers obtained drag-to-thrust conversion to boost the final thrust to $C_{T2}=0.124$ and $C_{T3}=0.181$ respectively. The thrust on the 3rd swimmer achieved by equal weight in $\mathcal J$ was merely slightly lower than controlling the 3rd swimmer only, showing that w=[0,0.5,0.5] was a better choice for both following swimmers.

With the optimal motion, the horizontal force profile in one period was also changed dramatically for following swimmers, as plotted in figure 5. Initially with synchronous undulation, C_{Fx} was almost steady. However, after the optimization it became highly unsteady with bigger magnitudes, which implies drastic change has also taken place in the flow field. When only controlling the force of the 3rd swimmer, the 2nd swimmer still experienced net drag in one period, while the 3rd swimmer spent over half of the period experiencing negative C_{Fx} , which resulted in the net thrust over one period. When having equal weight for both following swimmers, the 2nd swimmer had a significantly different force profile with much time having negative C_{Fx} . The force profile of the 3rd swimmer overall had the similar shape to the previous case, with larger peak and valley values of C_{Fx} .

The flow structures before and after the optimization are shown in figure [6]. It can be seen that strong vortex shedding was induced by heaving motion and undulating with different wave lengths after the optimization for both weight settings. Leading edge vortices (LEVs) were generated on both 2nd and 3rd swimmer, and were strengthened by the wake of the leading swimmer. Active and complex vortex pairing occurred in the wake of the 3rd swimmer. There was not only the interaction between the LEV and the trailing edge vortex (TEV) of the 3rd swimmer, but also the vortex shed from the 2nd swimmer intertwining with vortices separated from the 3rd swimmer. When the 2nd swimmer was not optimized, the very short wave length of its undulation had negative impact on the LEV shedding, making it noticeably less intense, which might impede the interaction with the wake of the leading swimmer, and eventually hamper its own hydrodynamic performance in terms of the drag. When both swimmers were controlled, they moved with similar pace to generate strong LEVs. The suction effect brought by these more active LEVs may contribute greatly to the thrust enhancement.

Based on the motion optimization results, the formation of the following swimmers were further optimized. Here only $\mathbf{w} = [0, 0.5, 0.5]$ was studied, considering it was able to achieve drag-to-thrust conversion for both following swimmers. The optimization started right with the optimal motion obtained in the previous control, with $A_2 = 0.89$, $A_3 = 1.0$, $\lambda_2 = 0.61$, and $\lambda_3 = 1.65$ being fixed for the formation control. Therefore, the control vector can be written

as $\gamma_i = [\delta x_i, \delta y_i]$ where i = 2, 3. It can be seen that formation control can effectively keep minimizing the objective function including C_{Fx} for both following swimmers based on the optimal motion. The overall thrust of following swimmers increased by 37.5%, with C_{T2} increased to 0.229 and C_{T3} to 0.212. As seen in figure $\frac{4}{9}$ (h), the 2nd swimmer was located farther from the leading swimmer by 0.47c, and was moved downward by 0.065c from its equilibrium position. The 3rd swimmer was also positioned backward by 0.091c, and was moved downward by 0.095c from its equilibrium position. The most significant formation change occurred to the horizontal position of the 2nd swimmer, which led to big alterations in horizontal force profile too as shown in figure $\frac{5}{9}$ (c).

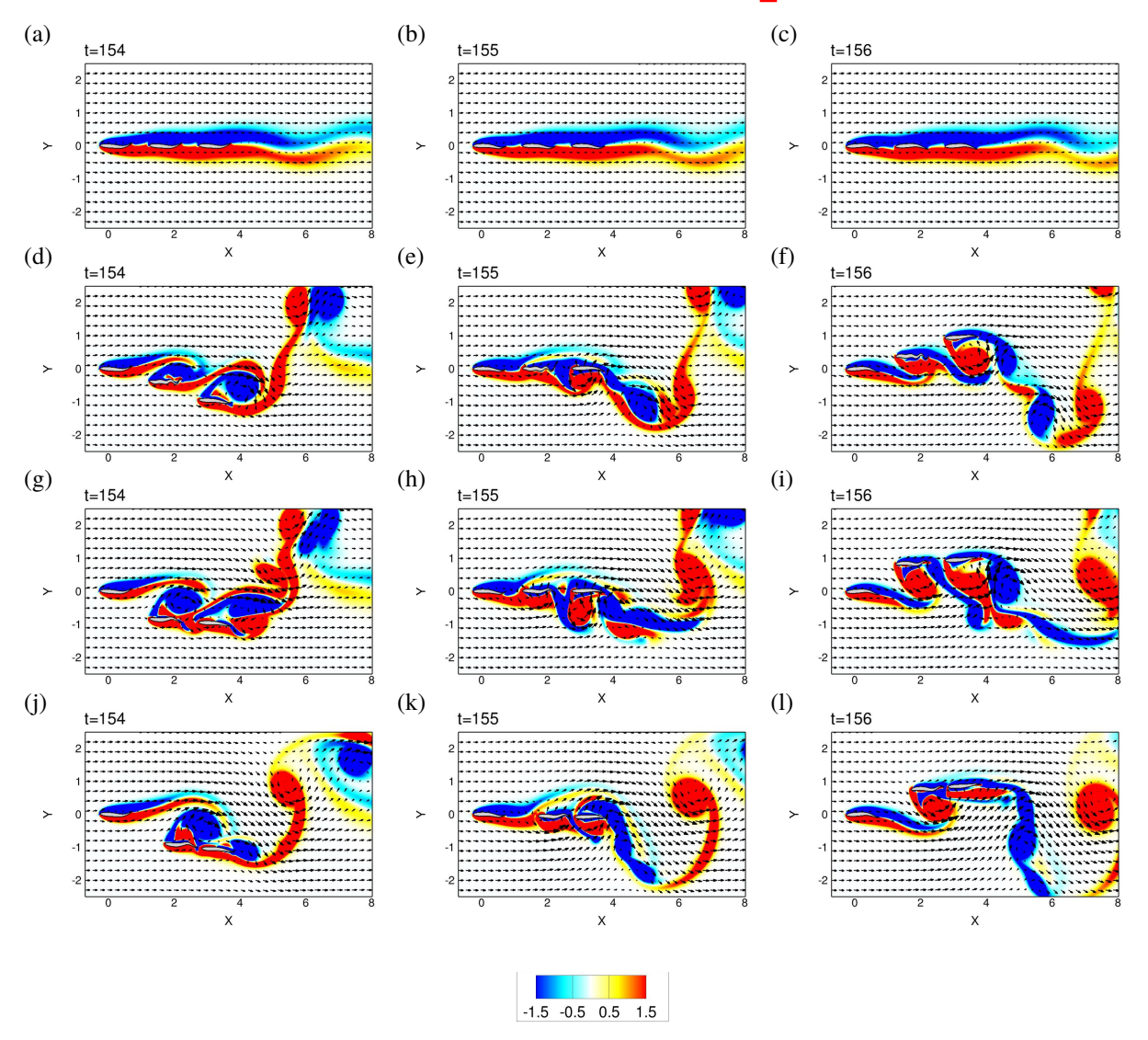


Fig. 6 The flow fields at three typical time moments contoured by vorticity. (a – c): The initial flow; (d – f): the optimal flow after optimization on $\gamma_i = [A_i, \lambda_i]$ with w = [0, 0, 1]; (g – i): the optimal flow after optimization on $\gamma_i = [A_i, \lambda_i]$ with w = [0, 0.5, 0.5]; (j – l): the optimal flow after optimization on $\gamma_i = [\delta x_i, \delta y_i]$ with w = [0, 0.5, 0.5]. Black arrows indicate the velocity vectors.

As presented in figure 5 (c), much lower minimal C_{Fx} values were achieved on the 2nd swimmer, which were approximately two times the minimal C_{Fx} after motion optimization. Peak values of C_{Fx} were increased as well, nevertheless the change of force profile still contributed to 59.0% enhancement of mean thrust on the 2nd swimmer. Contrary to the 2nd swimmer, the amplitude of C_{Fx3} became smaller after the optimization on position, but the average thrust in one undulating period still managed to increase by 14.6% when both following swimmers were positioned in the optimal manner.

The flow structures after the formation optimization at the same time moments are shown in figure [6](j-1). It can be seen that the vortex structures were quite different than the ones shown in figure [6](g-i) due to the change of distance between swimmers. The impact of the vortices shed from the leading swimmer was weaker when both following swimmers were placed farther into the downstream. The LEV of the 2nd swimmer had higher intensity to provide more suction ahead of the solid body, resulting in stronger thrust. Smaller distance between two following swimmers made them interact with the wake as a single moving bluff body, inducing a single vortex street instead of the complicated vortex pairing after optimization on the motion. It can be inferred that for the following swimmers, moving as one swimmer and closer the spacing between them to depress the vortex generated in the gap may contribute to the mean thrust enhancement.

B. Four swimmers in diamond formation

In this section, four flexible swimmers were initially positioned in diamond formation, performing the same harmonic undulation as prior section, as illustrated in figure Γ (b) with horizontal spacing L=0.5c and vertical spacing H=c. The Reynolds number remained 200. The swimmers were also able to heave periodically in vertical direction. Similar to the prior section, the control was performed on motion first, then followed by an optimization on the position based on optimal motion. Both optimizations aimed at optimizing the horizontal force on all following swimmers, therefore the weight for three following swimmers in \mathcal{J} was set equally as $\mathbf{w} = [0, 1/3, 1/3, 1/3]$. For the initial synchronous undulation, all four swimmers had the same $\gamma_i^{(0)} = [0, 1.0]$. A snapshot of the initial flow field is presented in figure $\overline{\mathcal{J}}$. Same constraints were imposed to A_i and λ_i during the motion optimization as prior case. All force coefficients were averaged in one undulating period with T=5. With only undulating motion, initially normal wake structures were formed without vortex-structure interactions. In this condition, all following swimmers were experiencing net mean drag as $C_{\overline{D}2} = 0.300$, $C_{\overline{D}3} = 0.300$, and $C_{\overline{D}4} = 0.197$. Note that by swimming in the wake of the 1st swimmer, the 4th swimmer already had lower drag than other swimmers.

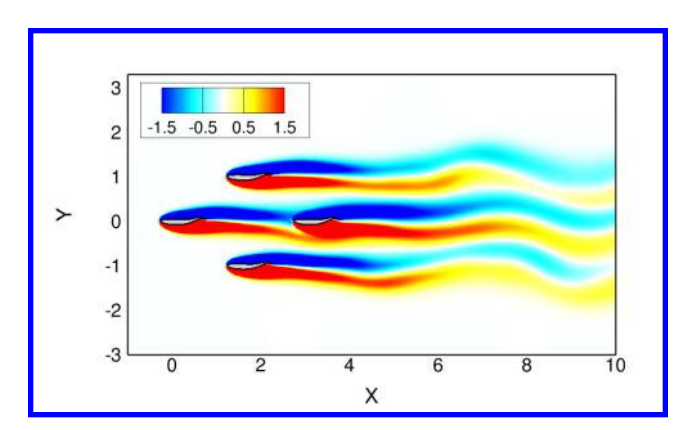


Fig. 7 The initial flow field of quadruple flexible swimmers undulating synchronously in diamond formation, contoured by vorticity.

The variations of \mathcal{J} and γ_i during the motion optimization are shown in figure (a-d). It can be seen that for all three followers, the mean drag was effectively reduced by the motion optimization. Moreover, drag-to-thrust conversion was achieved on the 4th swimmer, with C_{D4} reduced by 150% to a net thrust equal to $C_{D4} = 0.098$. C_{D2} and C_{D3} were decreased by 10.3% and 51.1% respectively. The heaving amplitude of three following swimmers was all increased significantly, as $|A_2| = 0.42$, $|A_3| = 1.0$, and $|A_4| = 0.96$. Note that optimal A_3 and A_4 almost reached the upper limits for the control. The wave length of the undulation changed differently, with λ_2 and λ_4 decreased by 20.9% and 30.2% respectively, and λ_3 increased by 52.7%. Based on the motion optimization results, the formation of the following swimmers were further optimized. The optimization started right with the optimal $\gamma_i = [A_i, \lambda_i]$, and they were fixed during the formation control. Therefore, the control vector was constructed as $\gamma_i = [\delta x_i, \delta y_i]$ where i = 2, 3, 4. The variation of the objective function as well as new γ_i is shown in figure (e - h). It is found that the formation control further reduced the horizontal force on three following swimmers effectively. C_{D2} was decreased by 10.5%, and C_{D3} was decreased by 33.8%. The mean thrust on the 4th swimmer was enhanced significantly by 59.6% to $C_T = 0.157$. As indicated in figure (f - h), all following swimmers were positioned backward in horizontal direction, as the 2nd swimmer was located farther by 0.27c, the 3rd swimmer by 0.61c, and the 4th swimmer by 0.58c respectively from

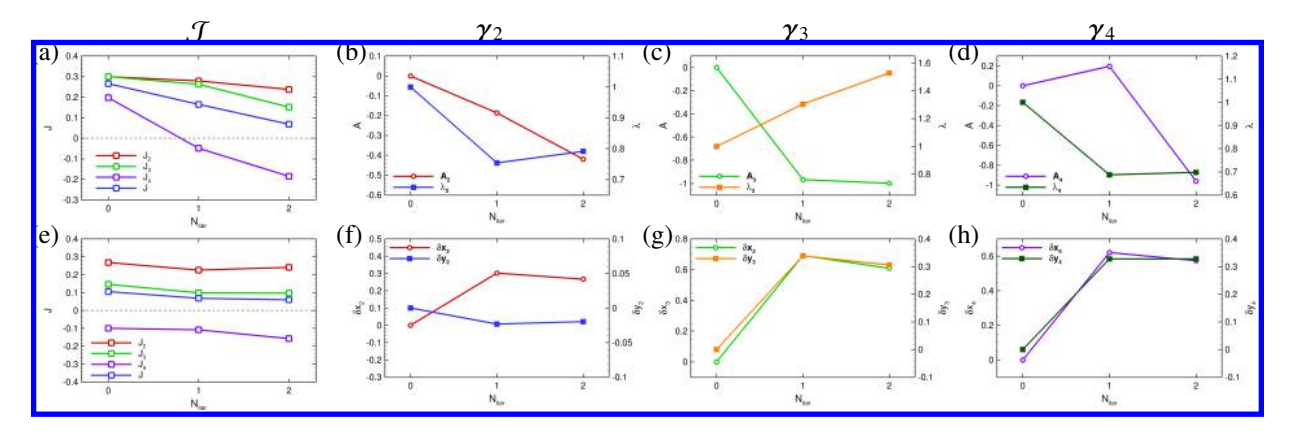


Fig. 8 The variations of objective function \mathcal{J} (the first column from the left), γ_2 (the second column), γ_3 (the third column), and γ_4 (the forth column) with respect to optimization iterations. (a – d): motion optimization with $\gamma_i = [A_i, \lambda_i]$; (e – h): formation optimization with $\gamma_i = [\delta x_i, \delta y_i]$.

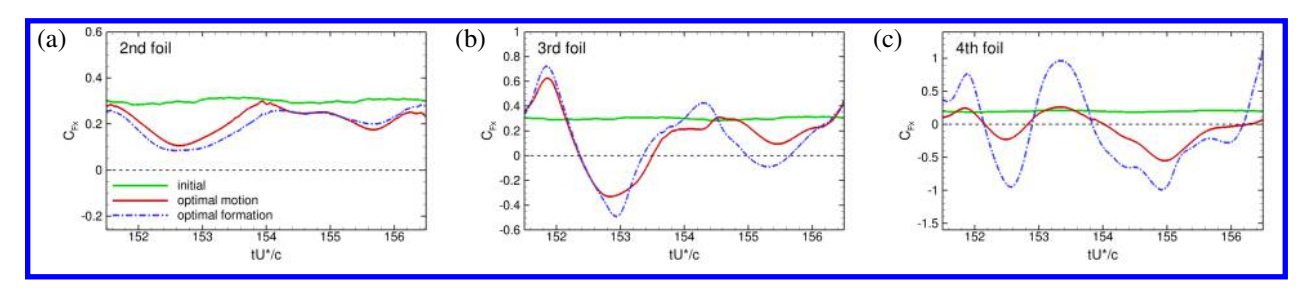


Fig. 9 The horizontal force coefficient profile in one undulating period before and after motion and formation optimization for the 2nd (a), the 3rd (b), and the 4th (c) swimmer.

their equilibrium positions. In terms of the change in vertical direction, the 2nd swimmer was positioned downward slightly by 0.02c, while the 3rd and the 4th swimmer were both moved upward by 0.31c and 0.33c respectively.

Corresponding to the optimal motion and formation, the horizontal force profile in one period after the optimization was changed dramatically for following swimmers, as plotted in figure Q. Initially with synchronous undulation, C_{Fx} was almost steady for all swimmers as previous triple-swimmer case. After the optimization of motion, C_{Fx} became highly unsteady with larger magnitudes. The entire C_{Fx} profile shifted down with its peak value lower than the original C_{D2} , while its minimum value was still greater than 0, resulting in a lower mean drag. For the 3rd and 4th swimmer, negative instantaneous C_{Fx} was achieved after motion optimization.

The change in force profiles is closely related to the change of flow structures. Figure $\boxed{10}$ presents the flow structures before and after the optimization at three typical time moments. It can be seen in figure $\boxed{10}$ (d –f) that after the motion optimization, separating vortices started to form on the following swimmers. The vortices were induced again by triggering heaving motion and modifying the wave length of undulation. The diamond formation complicated the interaction between vortices. The wake of the leading swimmer was found merging into the LEVs on the 2nd and 3rd swimmer, which strengthened those LEVs. Due to the existence of the 4th swimmer, the vortices shed from the 2nd and the 3rd swimmer could not form a stable wake. Instead, these vortices were further interacting and merging with the separating vortex on the 4th swimmer, leading to more complex and stronger vortices as seen in figure $\boxed{0}$ (e) and (f). Comparing to figure $\boxed{0}$ (c), it is found that a maximum instantaneous thrust was reached on the 4th swimmer when a strong LEV was formed and interacting with the vortices shed from the swimmer ahead of it, creating a suction effect by these more active vortices to contribute greatly to the thrust enhancement. However, when the wake of leader impinged directly on the 4th swimmer, it would experience net drag, as at t = 153 and 154.

The flow fields after the formation optimization are shown in figure $\boxed{10}$ (g – i). By moving backward, the vortex structures almost remained the same for the 2nd swimmer, which is corresponding to a slight reduction on its drag. By moving backward more and upward by 0.31c, the 3rd swimmer had wider horizontal space between itself and the leader, allowing the 3rd swimmer to avoid the direct impingement of the vortices shed from ahead, while inducing more active vortex interactions in its own wake. The change in vortex structures may further reduce the mean drag. For the 4th

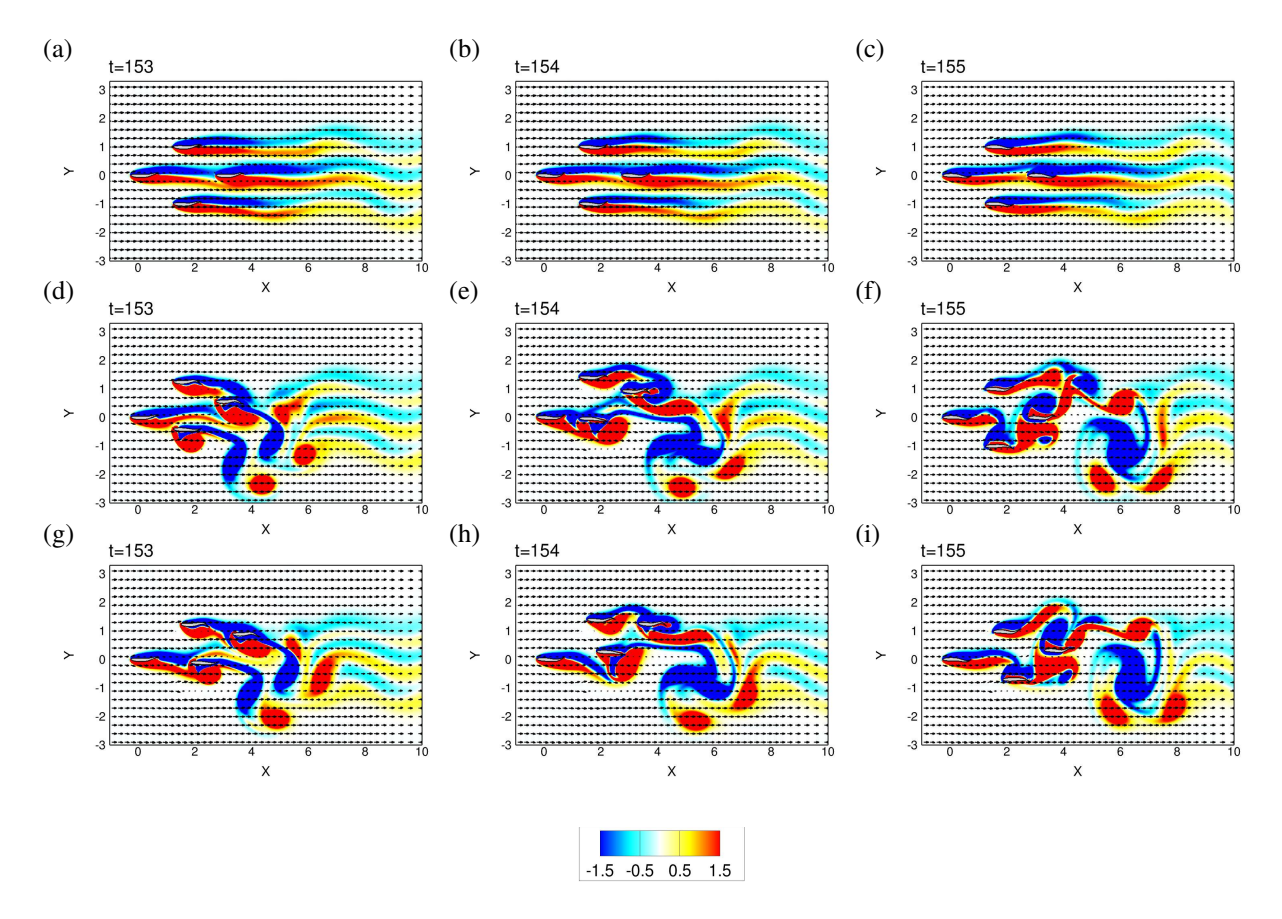


Fig. 10 The flow fields at three typical time moments contoured by vorticity. (a – c): The initial flow; (d – f): the optimal flow after optimization on motion with $\gamma_i = [A_i, \lambda_i]$; (g – i): the optimal flow after optimization on formation with $\gamma_i = [\delta x_i, \delta y_i]$. Black arrows indicate the velocity vectors.

swimmer, more difference in vortex structures can be observed especially in the near-solid area after relocating it. After the optimal formation, the 4th swimmer was actually closer to the swimmers ahead, leading to stronger interactions between the LEV and the wake ahead. As a result, the lift profile became more fluctuated as presented in figure 9 (c), but the stronger suction effect also boosted the mean thrust.

IV. Concluding Remarks

In this paper, an adjoint-based approach has been developed and applied to the optimization of hydrodynamic performance of flexible swimmers in school. The schooling was optimized with respect to the drag on the following swimmers by controlling the motion and formation of them. The optimization was performed under modest Reynolds number equal to 200. The periodic heaving and undulating motion were controlled for the motion, and the position was controlled for the formation. Triple swimmers in tandem and quadruple swimmers in a diamond formation were both studied. All swimmers were undulating in carangiform synchronously before the optimization to mimic the schooling behavior.

For triple swimmers in tandem formation, drag-to-thrust conversion was achieved first by motion optimization when both following swimmers were weighted equally. It was found to be beneficial for thrust enhancement to increase the heaving amplitude of both swimmers thus making them oscillating more synchronously in vertical direction. As for the undulating motion, the 2nd swimmer decreased its wave length while the 3rd swimmer increased the wave length for better thrust production. Based on the optimal motion, the optimization on the position further boosted the thrust to move the 2nd and 3rd swimmers farther from the leader, while positioning themselves closer. The optimal formation was able to strengthen the LEV of the 2nd swimmer to generate more suction effect, while decreasing the vortex interaction between the following swimmers for a more coherent vortex structure in the wake.

For quadruple swimmers in diamond formation, equal weight was imposed to all three following swimmers. It was found that the motion optimization was able to effectively reduced the drag on the 2nd and the 3rd swimmer, while the 4th swimmer achieved a drag-to-thrust conversion. The heaving motion was triggered for the generation of separation vortices, while the wave length of the undulation was tuned for better hydrodynamic performance as well. The further formation optimization moved the 2nd and the 3rd swimmer backward, which slightly changed the drag force profile of them, leading to overall lower mean drag. The 4th swimmer was positioned closer to the swimmers ahead, and its horizontal force profile experienced much stronger fluctuation due to more active interactions between the LEV and the wake of swimmers ahead, which resulted in extra boost in the mean thrust. It is crucial for the thrust enhancement by avoiding the direct impingement of the vortices from leading swimmers and taking advantage of the suction effect from the vortex interaction.

Acknowledgments

BX thanks the support from Army Research Laboratory (ARL) Research Associate Program (RAP) administered by Oak Ridge Associated Universities (ORAU) through W911NF-21-2-0178. MW thanks the support by NSF-CBET with grant number 2328027. This research was conducted at Kansas State University and all DEVCOM ARL contributions have been approved for public release.

References

- [1] Weihs, D., "Hydromechanics of fish schooling," Nature, Vol. 241, No. 5387, 1973, pp. 290–291.
- [2] Gopalkrishnan, R., Triantafyllou, M. S., Triantafyllou, G. S., and Barrett, D., "Active vorticity control in a shear flow using a flapping foil," *Journal of Fluid Mechanics*, Vol. 274, 1994, pp. 1–21.
- [3] Liao, J. C., "A review of fish swimming mechanics and behaviour in altered flows," *Philosophical Transactions of the Royal Society B: Biological Sciences*, Vol. 362, No. 1487, 2007, pp. 1973–1993.
- [4] Liao James, C., Beal David, N., Lauder George, V., and Triantafyllou Michael, S., "Fish exploiting vortices decrease muscle activity," *Science*, Vol. 302, No. 5650, 2003.
- [5] Marras, S., and Porfiri, M., "Fish and robots swimming together: attraction towards the robot demands biomimetic locomotion," *Journal of The Royal Society Interface*, Vol. 9, No. 73, 2012, pp. 1856–1868.
- [6] Li, L., Nagy, M., Graving, J. M., Bak-Coleman, J., Xie, G., and Couzin, I. D., "Vortex phase matching as a strategy for schooling in robots and in fish," *Nature Communications*, Vol. 11, No. 1, 2020, p. 5408.
- [7] Filella, A., Nadal, F., Sire, C., Kanso, E., and Eloy, C., "Model of Collective Fish Behavior with Hydrodynamic Interactions," *Physical Review Letters*, Vol. 120, No. 19, 2018, p. 198101.
- [8] Lauder, G. V., "Fish locomotion: recent advances and new directions," Annual Review of Marine Science, Vol. 7, No. 1, 2015, pp. 521–545.
- [9] Gao, A., and Triantafyllou, M. S., "Independent caudal fin actuation enables high energy extraction and control in two-dimensional fish-like group swimming," *Journal of Fluid Mechanicss*, Vol. 850, 2018, pp. 304–335.
- [10] Park, S. G., and Sung, H. J., "Hydrodynamics of flexible fins propelled in tandem, diagonal, triangular and diamond configurations," *Journal of Fluid Mechanics*, Vol. 840, 2018, pp. 154–189.
- [11] Pan, Y., and Dong, H., "Computational analysis of hydrodynamic interactions in a high-density fish school," *Physics of Fluids*, Vol. 32, No. 12, 2020, p. 121901.
- [12] Han, P., Lauder, G. V., and Dong, H., "Hydrodynamics of median-fin interactions in fish-like locomotion: Effects of fin shape and movement," *Physics of Fluids*, Vol. 32, No. 1, 2020.
- [13] Yu, H., Lu, X.-Y., and Huang, H., "Collective locomotion of two uncoordinated undulatory self-propelled foils," *Physics of Fluids*, Vol. 33, No. 1, 2021, p. 011904.
- [14] Hemelrijk, C. K., Reid, D. A. P., Hildenbrandt, H., and Padding, J. T., "The increased efficiency of fish swimming in a school," *Fish and Fisheries*, Vol. 16, No. 3, 2015, pp. 511–521.

- [15] Daghooghi, M., and Borazjani, I., "The hydrodynamic advantages of synchronized swimming in a rectangular pattern," *Bioinspiration & Biomimetics*, Vol. 10, No. 5, 2015, p. 056018.
- [16] Ji, T., Jin, F., Xie, F., Zheng, H., Zhang, X., and Zheng, Y., "Active learning of tandem flapping wings at optimizing propulsion performance," *Physics of Fluids*, Vol. 34, No. 4, 2022, p. 047117.
- [17] Mittal, R., Dong, H., Bozkurttas, M., Najjar, F., Vargas, A., and Von Loebbecke, A., "A versatile sharp interface immersed boundary method for incompressible flows with complex boundaries," *Journal of Computational Physics*, Vol. 227, No. 10, 2008, pp. 4825–4852.
- [18] Fadlun, E. A., Verzicco, R., Orlandi, P., and Mohd-Yusof, J., "Combined immersed-boundary finite-difference methods for three-dimensional complex flow simulations," *Journal of Computational Physics*, Vol. 161, No. 1, 2000, pp. 35–60.
- [19] Yang, T., Wei, M., and Zhao, H., "Numerical study of flexible flapping wing propulsion," AIAA Journal, Vol. 48, No. 12, 2010, pp. 2909–2915.
- [20] Xu, M., Wei, M., Yang, T., and Lee, Y. S., "An embedded boundary approach for the simulation of a flexible flapping wing at different density ratio," *European Journal of Mechanics-B/Fluids*, Vol. 55, 2016, pp. 146–156.
- [21] Xu, M., and Wei, M., "Using adjoint-based optimization to study kinematics and deformation of flapping wings," *Journal of Fluid Mechanics*, Vol. 799, 2016, pp. 56–99.
- [22] Xu, B., Colgan, D., Wei, M., and Hrynuk, J. T., *Adjoint-Based Optimal Control on Flows with Multiple Moving Cylinders in Tandem*, AIAA SciTech Forum, American Institute of Aeronautics and Astronautics, 2023.
- [23] Colgan, D., Xu, B., Wei, M., and Hrynuk, J., 3D vortical structure of multiple moving spheroids under adjoint-based optimal control, AIAA SciTech Forum, American Institute of Aeronautics and Astronautics, 2023.
- [24] Di Santo, V., Goerig, E., Wainwright Dylan, K., Akanyeti, O., Liao James, C., Castro-Santos, T., and Lauder George, V., "Convergence of undulatory swimming kinematics across a diversity of fishes," *Proceedings of the National Academy of Sciences*, Vol. 118, No. 49, 2021, p. e2113206118.
- [25] Khalid, M. S. U., Wang, J., Dong, H., and Liu, M., "Flow transitions and mapping for undulating swimmers," *Physical Review Fluids*, Vol. 5, No. 6, 2020, p. 063104.
- [26] Videler, J., and Hess, F., "Fast continuous swimming of two pelagic predators, saithe (Pollachius virens) and mackerel (Scomber scombrus): a kinematic analysis," *Journal of Experimental Biology*, Vol. 109, No. 1, 1984, pp. 209–228.